Research Square

Preprints are preliminary reports that have not undergone peer review.
They should not be considered conclusive, used to inform clinical practice,
or referenced by the media as validated information.

Apelin-13 attenuates experimental sepsis-associated myocardial injury in association with reduced endoplasmic reticulum stress and mitochondrial dysfunction

Qing Song
The First Affiliated Hospital of Dalian Medical University
Youxiong Zhao
The First Affiliated Hospital of Dalian Medical University
Jiuqing Li
The First Affiliated Hospital of Dalian Medical University
Zhiyao Fang
The First Affiliated Hospital of Dalian Medical University
Suwei Li
lisuweicn@163.com
The First Affiliated Hospital of Dalian Medical University

Research Article

Keywords: Apelin-13, sepsis, myocardial injury, endoplasmic reticulum stress, mitochondrial dysfunction

Posted Date: November 12th, 2026

DOI: https://doi.org/10.21203/rs.3.rs-11476411/v1

License: This work is licensed under a Creative Commons Attribution 4.0 International License.
Read Full License

Additional Declarations: No competing interests reported.

Abstract

Sepsis-associated myocardial injury is driven by interacting inflammatory, oxidative, endoplasmic reticulum (ER), and mitochondrial stress responses. This study investigated whether Apelin-13 protects against myocardial injury during experimental sepsis. Male Sprague-Dawley rats were assigned to sham-operated control, cecal ligation and puncture (CLP), or CLP plus Apelin-13 groups. Apelin-13 was administered intraperitoneally after CLP, and blood and myocardial tissues were collected at 48 h. In parallel, H9c2 cardiomyoblasts were pretreated with Apelin-13 before lipopolysaccharide challenge. CLP caused myocardial histopathological injury, inflammatory cell infiltration, increased circulating interleukin-1β and tumor necrosis factor-α, and increased myocardial GRP78, MLKL, and cleaved caspase-3 immunoreactivity. These changes were attenuated by Apelin-13. In H9c2 cells, Apelin-13 improved viability, reduced lactate dehydrogenase release, decreased GRP78, PERK, CHOP, Bax, and cleaved caspase-3 abundance, and restored Bcl-xL expression. Apelin-13 also reduced intracellular and mitochondrial reactive oxygen species and partially preserved mitochondrial membrane potential. Thus, Apelin-13 attenuated experimental sepsis-associated myocardial and cardiomyoblast injury, an effect associated with reduced inflammation and ER stress and improved mitochondrial homeostasis.

Introduction

Sepsis is a life-threatening organ dysfunction caused by a dysregulated host response to infection and remains a major global health burden [1]. The latest comprehensive global analysis estimated that 48.9 million cases of sepsis and 11.0 million sepsis-related deaths occurred worldwide in 2017, accounting for approximately 20% of all global deaths [2]. Cardiac involvement is common during sepsis, and sepsis-induced myocardial dysfunction (SIMD), also referred to as septic cardiomyopathy, may aggravate hemodynamic instability and adversely affect clinical outcomes [3]. The reported prevalence of SIMD ranges from 10% to 70%, largely because of differences in diagnostic criteria, assessment methods, timing of evaluation, and cardiac loading conditions among studies [4]. A recent systematic review and meta-analysis estimated a pooled prevalence of approximately 20% and demonstrated that SIMD was associated with increased short-term mortality [5]. Although dysregulated inflammation, oxidative stress, mitochondrial dysfunction, metabolic disturbance, and multiple forms of regulated cardiomyocyte death have been implicated in the development of SIMD, its underlying molecular mechanisms remain incompletely understood [6]. Therefore, elucidating the mechanisms of sepsis-associated myocardial injury and identifying effective cardioprotective interventions remain important research priorities.

Apelin was originally identified as an endogenous peptide ligand for the G protein-coupled receptor APJ, which is now termed the apelin receptor [7]. Post-translational processing of preproapelin generates several active isoforms, among which Apelin-13 exhibits potent biological activity [8]. The apelinergic system regulates myocardial contractility, vascular tone, angiogenesis, fluid homeostasis, and energy metabolism through context-dependent receptor signaling [9]. It also modulates inflammatory and

oxidative responses in cardiovascular and systemic inflammatory disorders [10]. These properties have led to increasing interest in the apelin/APJ system as a potential therapeutic target in sepsis [11].

Experimental evidence supports a protective role for apelin in septic cardiac injury. An early study demonstrated that exogenous apelin attenuated myocardial impairment and inflammatory responses in septic rats [12]. Apelin was subsequently shown to provide greater cardioprotection and prolong survival compared with dobutamine in a rat model of endotoxin-induced myocardial dysfunction [13]. In a cecal ligation and puncture(CLP) model, apelin reduced myocardial injury in association with inhibition of TLR4- and NLRP3-related inflammatory signaling [14]. Apelin-13 also stabilized cardiorenal hemodynamics in ovine septic shock, although enhanced peptide degradation in plasma from patients with sepsis may limit clinical translation [15]. More recent work associated the myocardial effects of apelin with suppression of NLRP3-mediated cardiomyocyte pyroptosis [16]. In addition, repeated Apelin-13 administration reduced norepinephrine requirements in rats subjected to CLP [17]. Nevertheless, whether its cardioprotection is accompanied by coordinated improvements in endoplasmic reticulum (ER) stress, mitochondrial dysfunction, oxidative injury, and cardiomyocyte death remains incompletely defined.

The ER and mitochondria form an interconnected stress-response network in metabolically active cardiomyocytes. ER stress is increasingly recognized as an important component of sepsis-associated organ injury [18]. The unfolded protein response initially promotes adaptation, but prolonged activation may shift signaling toward inflammation and cell death [19]. In CLP-treated rats, myocardial ER stress has been associated with activation of apoptosis-related pathways [20]. In lipopolysaccharide (LPS)-challenged H9c2 cells, reactive oxygen species(ROS) can amplify ER stress and apoptosis, supporting functional interaction between oxidative and proteotoxic stress [21]. Necroptosis represents another regulated cell-death program involving RIPK1, RIPK3, and mixed lineage kinase domain-like protein (MLKL) [22]. Phosphorylated MLKL can disrupt plasma membrane integrity, although its measurement alone does not establish definitive necroptotic death [23].

The present study aimed to investigate whether Apelin-13 attenuates sepsis-associated myocardial injury and whether its protective effects are associated with suppression of GRP78/PERK/CHOP-related ER stress and preservation of mitochondrial homeostasis. These effects were evaluated in a rat model of CLP-induced sepsis and in LPS-challenged H9c2 cells. The findings may provide experimental evidence supporting Apelin-13 as a potential therapeutic candidate for sepsis-associated myocardial injury.

Materials and methods

Animals and ethical approval

A total of 18 male Sprague-Dawley rats, aged 6–8 weeks and weighing approximately 220 g, were obtained from Liaoning Changsheng Biotechnology Co., Ltd. (China). The animals were housed in a

specific pathogen-free facility at the Laboratory Animal Center of Dalian Medical University under controlled environmental conditions with a 12-h light/dark cycle and free access to standard laboratory chow and water. The sample size was determined based on previous studies and preliminary experiments. All animal procedures were approved by the Institutional Animal Care and Use Committee of Dalian Medical University (approval no. AEE23119) and were conducted in accordance with the approved protocols and institutional guidelines.

Cecal ligation and puncture model and experimental design

Sepsis-associated myocardial injury was induced using CLP. Rats were anesthetized by intraperitoneal injection of tribromoethanol at a dose of 300 mg/kg. After adequate anesthesia was confirmed, the abdominal area was shaved and disinfected, and a 2–3-cm midline incision was made. The cecum was gently exteriorized and ligated at the distal one-third using a 3 − 0 non-absorbable suture, while care was taken to avoid intestinal obstruction. The ligated cecum was punctured with an 18-gauge needle, and a small amount of fecal material was gently extruded through the puncture site to ensure patency. The cecum was then returned to the abdominal cavity, and the abdominal wall and skin were closed in layers.

The rats were randomly allocated using a random-number table to three groups, with six animals in each group: the Control (sham-operated) group, CLP group, and CLP + Apelin-13 group. Rats in the Control group underwent laparotomy and cecal exposure without ligation or puncture, whereas rats in the CLP and CLP + Apelin-13 groups underwent the complete CLP procedure. Apelin-13 (Selleck Chemicals LLC, USA; catalog no. P1211; purity, 99.74% by high-performance liquid chromatography) was administered intraperitoneally at 20 mg/kg beginning 12 h after CLP. Subsequent injections were administered at 17, 22, 27, 32, 37, and 42 h after surgery. Rats in the Control and CLP groups received an equivalent volume of sterile saline at the corresponding time points. Blinding was not feasible for investigators performing the surgical procedures and administering the treatments because they were aware of group allocation. However, investigators responsible for outcome assessment and data analysis were blinded to group allocation. All surviving animals were euthanized 48 h after surgery, and blood and myocardial tissue samples were collected for subsequent analyses.

Blood and myocardial tissue collection

At 48 h after surgery, rats were deeply anesthetized and placed in the supine position. The abdominal aorta was carefully exposed, and approximately 5 mL of arterial blood was collected. Following blood collection, the rats were euthanized by cervical dislocation while under deep anesthesia. Blood samples were maintained at room temperature for 30 min to allow clotting and subsequently centrifuged at 1,500 rpm for 15 min. The resulting serum was collected and stored at -80°C until analysis.

The thoracic cavity was then opened, and the heart was perfused through the left ventricle with ice-cold sterile saline until the perfusate from the right ventricle became clear. The heart was rapidly excised and

washed with pre-cooled saline. A portion of the myocardial tissue was fixed in 4% paraformaldehyde for histological and immunohistochemical analyses, whereas the remaining tissue was snap-frozen in liquid nitrogen and stored at − 80°C.

Enzyme-linked immunosorbent assay

Serum concentrations of tumor necrosis factor-α and interleukin-1β were measured using rat ELISA kits (Elabscience Biotechnology Co., Ltd., Wuhan, China) according to the manufacturer's instructions. Absorbance was measured using a microplate reader, and cytokine concentrations were calculated from the corresponding standard curves. Six independent serum samples from six rats were analyzed in each group.

Histological examination

Myocardial tissues fixed in 4% paraformaldehyde were dehydrated through a graded ethanol series, cleared in xylene, embedded in paraffin and cut into 3–5-μm sections. The sections were deparaffinized, rehydrated and stained with hematoxylin for 10 min. After differentiation in 0.1% hydrochloric acid–ethanol solution, the sections were counterstained with eosin for 2 min. The sections were then dehydrated, cleared and mounted with neutral resin.

Myocardial histopathological injury was evaluated using a study-defined semiquantitative scoring system comprising myocardial fiber disorganization or disruption, interstitial edema, and inflammatory cell infiltration. Each feature was scored according to the proportion of evaluable myocardial tissue affected: 0, absent; 1, > 0–25%; 2, > 25–50%; 3, > 50–75%; and 4, > 75%. The three component scores were summed to obtain a total score ranging from 0 to 12 for each field. Three randomly selected, non-overlapping fields per animal were assessed at ×200 magnification. Regions containing tissue folds, tears, or other processing artifacts were excluded. The mean total score across the three fields was used as the histological injury score for each animal. Assessment was performed with the investigator blinded to group allocation.

Inflammatory cell infiltration was quantified by manually counting morphologically identifiable inflammatory cells within the myocardial interstitium using the Cell Counter plugin in ImageJ. Identification was based on cell size, nuclear-to-cytoplasmic ratio, nuclear morphology, and staining characteristics. Recognizable cardiomyocyte, endothelial, and fibroblast nuclei, intravascular cells, erythrocytes, and cells of uncertain identity were excluded. Three randomly selected, non-overlapping fields of equal area per animal were evaluated at ×200 magnification. Cells intersecting the upper or left field boundaries were included, whereas those intersecting the lower or right boundaries were excluded. The mean count across the three fields represented one biological replicate. Counting was performed with the investigator blinded to group allocation.

Immunohistochemistry

Paraffin-embedded myocardial sections were deparaffinized in xylene and rehydrated through a graded ethanol series. Antigen retrieval was performed in sodium citrate buffer using microwave heating. Endogenous peroxidase activity was blocked with 3% hydrogen peroxide for 30 min at room temperature, after which the sections were blocked with 5% bovine serum albumin for 1 h.

The sections were incubated overnight at 4°C with primary antibodies against GRP78, MLKL, and cleaved caspase-3. After washing with PBS, the sections were incubated with the corresponding horseradish peroxidase-conjugated secondary antibodies for 1 h at room temperature. Immunoreactivity was visualized using 3,3'-diaminobenzidine, and nuclei were counterstained with hematoxylin. The sections were subsequently dehydrated, cleared, and mounted.

Images were acquired using identical microscope settings. Three non-overlapping fields were randomly selected from each section at ×200 magnification. The percentage of positively stained area was quantified using ImageJ. The mean of the three fields represented one biological replicate, and six animals were analyzed in each group.

Cell culture

Rat H9c2 cardiomyoblasts were obtained from Procell Life Science & Technology Co., Ltd. (Wuhan, China). Cells were cultured in high-glucose Dulbecco's modified Eagle's medium supplemented with 10% fetal bovine serum and 1% penicillin-streptomycin at 37°C in a humidified atmosphere containing 5% CO_2.

LPS-induced cardiomyoblast injury and experimental groups

To determine the appropriate concentration of LPS from Escherichia coli O111:B4 (Sigma-Aldrich, USA; catalog no. L2630), H9c2 cells were treated with 10, 100, 500, or 1,000 μg/mL LPS for 24 h, and cell viability was subsequently evaluated. Based on the cell-viability results, 100 μg/mL LPS was selected for subsequent experiments.

To determine the protective concentration of Apelin-13, cells were pretreated with 0.01, 0.1, 1, or 2 μM Apelin-13 for 2 h before exposure to 100 μg/mL LPS for 24 h. Based on the resulting cell viability, 2 μM Apelin-13 was selected for subsequent experiments.

For the principal experiments, H9c2 cells were divided into three groups: the Control group, LPS group and LPS + Apelin-13 group. Cells in the Control group were cultured under normal conditions. Cells in the LPS group were exposed to 100 μg/mL LPS for 24 h. Cells in the LPS + Apelin-13 group were pretreated with 2 μM Apelin-13 for 2 h and subsequently exposed to 100 μg/mL LPS for 24 h. Each cell experiment was independently repeated three times.

Cell viability assay

Cell viability was assessed using a Cell Counting Kit-8 assay (MedChemExpress, USA). H9c2 cells were seeded into 96-well plates at approximately 5 × 10^3 cells per well in 100 μL of culture medium and cultured for 24 h. The cells were then serum-starved for 18 h before receiving the indicated treatments.

Following treatment, 10 μL of CCK-8 reagent was added to each well, and the cells were incubated at 37°C for 2 h. Absorbance was measured at 450 nm using a microplate reader. Five technical replicate wells were included for each experimental condition, and their mean was used as the result of one independent experiment. The experiment was independently repeated three times.

Lactate dehydrogenase release assay

Cell membrane damage was evaluated by measuring lactate dehydrogenase release into the culture medium using a commercially available lactate dehydrogenase assay kit according to the manufacturer's instructions. Following the indicated treatments, the culture supernatants were collected and centrifuged to remove cellular debris. Absorbance was measured using a microplate reader, and lactate dehydrogenase release was calculated according to the manufacturer's protocol. The experiment was independently repeated three times.

Western blotting

Following the indicated treatments, H9c2 cells were washed with ice-cold PBS and lysed in RIPA buffer supplemented with phenylmethylsulfonyl fluoride at a ratio of 100:1. Cell lysates were incubated on ice for 30 min and then centrifuged at 12,000 rpm for 10 min at 4°C. The supernatants were collected, and total protein concentrations were determined using a bicinchoninic acid assay.

Equal amounts of protein, corresponding to 20 μg per lane, were separated using 10 or 12.5% SDS-PAGE and transferred onto polyvinylidene fluoride membranes at a constant current of 200 mA. The membranes were blocked with 5% non-fat milk prepared in Tris-buffered saline containing 0.1% Tween-20 for 2 h at room temperature.

The membranes were incubated overnight at 4°C with primary antibodies against GRP78, PERK, CHOP, cleaved caspase-3, Bax, Bcl-xL, and GAPDH. After three washes with Tris-buffered saline containing 0.1% Tween-20, the membranes were incubated with the corresponding horseradish peroxidase-conjugated secondary antibodies for 1 h at room temperature.

Protein bands were visualized using an enhanced chemiluminescence substrate and captured using a chemiluminescence imaging system. Band intensities were quantified using ImageJ software and normalized to GAPDH. Each western blot experiment was independently repeated three times.

Hoechst staining

Apoptotic nuclear morphological changes were evaluated using Hoechst 33342 staining. Following the indicated treatments, H9c2 cells were incubated with Hoechst 33342 staining solution at 37°C for 20–30 min. The staining solution was removed, and the cells were washed two or three times with PBS.

Fluorescence images were acquired using an inverted fluorescence microscope under identical acquisition settings. Cells exhibiting chromatin condensation, nuclear shrinkage or nuclear fragmentation were considered apoptotic. Three non-overlapping fields were randomly selected for each independent experiment. The mean value of the three fields was used as one biological replicate, and the experiment was independently repeated three times.

Intracellular reactive oxygen species measurement

Intracellular reactive oxygen species production was assessed using the fluorescent probe 2',7'-dichlorodihydrofluorescein diacetate. Following the indicated treatments, H9c2 cells were incubated with the working solution at 37°C in the dark according to the manufacturer's instructions. The cells were subsequently washed with PBS to remove excess probe.

Fluorescence images were acquired using an inverted fluorescence microscope with identical exposure settings for all groups. Fluorescence intensity was quantified using ImageJ software after background subtraction and expressed relative to the Control group. Three non-overlapping fields were analyzed for each independent experiment, and the mean value of the three fields was used as one biological replicate. The experiment was independently repeated three times.

Mitochondrial superoxide measurement

Mitochondrial superoxide production was assessed using MitoSOX Red. A 5-mM stock solution was prepared by dissolving 50 μg MitoSOX Red in 13 μl dimethyl sulfoxide. The stock solution was aliquoted and stored at − 20°C in the dark to avoid repeated freeze–thaw cycles. Immediately before use, the stock solution was diluted 1:1,000 in pre-warmed HBSS to obtain a final concentration of 5 μM.

Following the indicated treatments, H9c2 cells were incubated with 500 μL of MitoSOX working solution at 37°C for 10 min in the dark. The cells were then washed three times with pre-warmed HBSS for 5 min each. Fluorescence images were acquired using identical exposure settings. Mean fluorescence intensity was quantified using ImageJ software after background subtraction and expressed relative to the Control group. Three non-overlapping fields were analyzed for each independent experiment, and the mean value was used as one biological replicate. The experiment was independently repeated three times.

Mitochondrial membrane potential assay

Mitochondrial membrane potential was evaluated using a JC-1 assay kit. Following the indicated treatments, H9c2 cells were incubated with 500 μL of JC-1 working solution at 37°C for 20 min. The staining solution was removed, and the cells were washed twice with JC-1 staining buffer. Fresh culture medium was subsequently added before fluorescence imaging.

Red fluorescence represented JC-1 aggregates in mitochondria with preserved membrane potential, whereas green fluorescence represented JC-1 monomers following mitochondrial depolarization. Images were acquired using identical exposure settings for all groups. Mitochondrial membrane potential was expressed as the ratio of red to green fluorescence intensity. Three non-overlapping fields were analyzed for each independent experiment, and the mean value was used as one biological replicate. The experiment was independently repeated three times.

Statistical analysis

Statistical analyses were performed using GraphPad Prism version 9.0. Quantitative data are presented as the mean ± standard deviation. For animal experiments, each data point represents an individual animal, and six animals were included in each group. For cell experiments, each data point represents the mean value obtained from one independent biological experiment, and all cell experiments were independently repeated three times.

Comparisons among three or more groups were performed using one-way analysis of variance followed by Bonferroni's multiple-comparisons test. All statistical tests were two-sided, and $P < 0.05$ was considered to indicate a statistically significant difference.

Results

Apelin-13 attenuates CLP-induced myocardial histopathological injury

Compared with the control group, rats subjected to CLP exhibited marked myocardial structural abnormalities, including disorganized myocardial fibers, widened interstitial spaces, inflammatory cell infiltration, and interstitial erythrocyte extravasation. These histopathological alterations were visibly attenuated by Apelin-13 treatment. Consistently, the myocardial injury score and inflammatory cell infiltration were increased after CLP and were significantly reduced in the CLP + Apelin-13 group (Fig. 1).

Apelin-13 reduces systemic inflammation and myocardial stress- and cell-death-related protein expression in septic rats

Serum IL-1β and TNF-α concentrations were significantly increased in the CLP group compared with the control group. Apelin-13 treatment reduced the CLP-induced increases in both inflammatory mediators. Quantification of myocardial immunohistochemical staining further showed that the positive areas for GRP78, MLKL, and cleaved caspase-3 were increased after CLP and were reduced following Apelin-13 treatment (Fig. 2).

Selection of LPS and Apelin-13 concentrations and assessment of H9c2 cell injury

Exposure of H9c2 cells to increasing concentrations of LPS for 24 h produced a concentration-dependent reduction in cell viability. Pretreatment with Apelin-13 improved the viability of LPS-challenged cells, with the greatest protective effect observed at 2 μM under the tested conditions. Based on these findings, 100 μg/mL LPS and 2 μM Apelin-13 were selected for subsequent experiments. Moreover, LPS markedly increased LDH release, whereas Apelin-13 pretreatment significantly reduced this increase, indicating preservation of cell membrane integrity (Fig. 3).

Apelin-13 suppresses ER-stress-related protein expression in LPS-challenged H9c2 cells

Western blot analysis showed that LPS increased the protein abundance of GRP78, PERK, and CHOP compared with the control group. Apelin-13 pretreatment significantly reduced the LPS-induced increases in these ER-stress-related proteins (Fig. 4), indicating that the cytoprotective effect of Apelin-13 was accompanied by attenuation of the ER stress response.

Apelin-13 attenuates apoptosis-related alterations in LPS-challenged H9c2 cells

Hoechst staining revealed increased nuclear condensation and fragmentation in LPS-challenged H9c2 cells, whereas these changes were less evident following Apelin-13 pretreatment. LPS also increased Bax and cleaved caspase-3 abundance and decreased Bcl-xL abundance. Apelin-13 partially reversed these alterations (Fig. 5), consistent with reduced apoptosis-related signaling.

Apelin-13 reduces oxidative stress and preserves mitochondrial membrane potential in LPS-challenged H9c2 cells

LPS exposure markedly increased intracellular ROS fluorescence and mitochondrial superoxide generation, as assessed using ROS-sensitive fluorescence and MitoSOX staining, respectively. Both signals were significantly reduced by Apelin-13 pretreatment. In addition, LPS decreased the JC-1 red/green fluorescence ratio, consistent with loss of mitochondrial membrane potential. Apelin-13 partially restored the JC-1 ratio (Fig. 6), indicating preservation of mitochondrial membrane polarization in LPS-challenged cells.

Discussion

The present study yielded several principal findings. First, Apelin-13 attenuated myocardial histopathological abnormalities and reduced circulating pro-inflammatory cytokines in rats subjected to CLP. Second, Apelin-13 reduced inflammatory and oxidative responses associated with experimental sepsis. Third, Apelin-13 preserved cell viability and mitochondrial membrane potential while reducing apoptosis-related changes in LPS-challenged H9c2 cells. Finally, the protective effects of Apelin-13 were accompanied by reduced abundance of ER-stress-related proteins, including GRP78, PERK, and CHOP, and lower myocardial MLKL expression. Together, these findings suggest that Apelin-13 attenuates experimental sepsis-associated myocardial injury and that this protection is associated with reduced ER stress and preservation of mitochondrial homeostasis.

Sepsis-associated myocardial injury is a complex pathological process involving inflammatory dysregulation, oxidative stress, metabolic disturbance, mitochondrial dysfunction, and multiple forms of cardiomyocyte death [24]. These mechanisms do not occur independently but may interact to form a self-amplifying cycle that promotes myocardial damage during sepsis [25]. In the current study, CLP induced marked myocardial histopathological abnormalities and increased circulating IL-1β and TNF-α concentrations. Apelin-13 attenuated these changes, supporting its protective effects against myocardial injury and systemic inflammation in this experimental model. Nevertheless, sepsis-induced cardiomyopathy is clinically defined according to alterations in systolic and/or diastolic cardiac function, for which echocardiography remains the principal diagnostic method [26]. Because cardiac contractility, ventricular function, and hemodynamic parameters were not directly evaluated in the present study, the findings should be interpreted as attenuation of sepsis-associated myocardial injury rather than definitive improvement in sepsis-induced cardiomyopathy. Importantly, Apelin-13 administration was initiated 12 h after CLP rather than before septic challenge. Therefore, the present treatment schedule more closely reflects a therapeutic intervention than a prophylactic approach.

ER stress has increasingly been recognized as an important contributor to myocardial injury during sepsis. Under physiological conditions, GRP78 maintains ER protein-folding homeostasis by binding to unfolded protein response sensors. When ER stress becomes persistent, dissociation of GRP78 promotes activation of PERK and induction of CHOP, thereby shifting the unfolded protein response from an adaptive process toward pro-apoptotic signaling. Previous studies have demonstrated that attenuation of ER stress is accompanied by reduced myocardial inflammation, apoptosis, and cardiac injury in experimental sepsis [27]. Consistent with these observations, CLP increased myocardial GRP78 immunoreactivity, whereas LPS increased GRP78, PERK, and CHOP protein abundance in H9c2 cells. These changes were attenuated by Apelin-13. The involvement of Apelin-13 in ER homeostasis has also been reported in other models of cardiovascular injury. Apelin-13 was shown to protect against myocardial ischemia/reperfusion injury through downregulation of ER-dependent apoptotic signaling [28]. Similarly, apelin treatment ameliorated acute heart failure in rabbits in association with suppression of ER stress [29]. These findings prompted us to consider whether attenuation of ER stress contributes to the cardioprotective effect of Apelin-13 during sepsis. The concomitant reductions in myocardial injury and GRP78/PERK/CHOP-related signaling support this possibility.

Oxidative stress and mitochondrial dysfunction may represent additional mechanisms associated with the effects of Apelin-13. Cardiomyocytes have high energy requirements and are particularly vulnerable to disruption of mitochondrial homeostasis. Loss of mitochondrial membrane potential may impair ATP production, increase reactive oxygen species generation, and promote the release of pro-apoptotic factors. Apelin-13 has previously been reported to reduce myocardial oxidative injury and apoptosis through FoxO1-related signaling in myocardial ischemia/reperfusion injury [30]. Interactions between the apelin/APJ system and cellular redox regulation have also been described in a range of cardiovascular and inflammatory conditions [31]. In the present study, LPS exposure increased intracellular and mitochondrial ROS signals and decreased the JC-1 red-to-green fluorescence ratio in H9c2 cells. Apelin-13 attenuated these changes, indicating reduced oxidative stress and partial preservation of mitochondrial membrane potential. These findings are consistent with the emerging concept that mitochondrial quality control and metabolic homeostasis are important determinants of sepsis-associated cardiac injury [32]. Therapeutic approaches directed at mitochondrial dysfunction have consequently been proposed as potential strategies for sepsis-induced cardiomyopathy [33]. Experimental evidence has shown that preservation of mitochondrial function may reduce inflammasome activation and myocardial injury during sepsis [34]. Furthermore, inhibition of pyruvate dehydrogenase kinase 4 was reported to attenuate myocardial and mitochondrial injury in an experimental model of sepsis, emphasizing the relationship between disturbed energy metabolism and cardiac damage [35]. Taken together, these observations suggest that preservation of mitochondrial homeostasis may be an important component of Apelin-13-associated cardioprotection.

The improvement in mitochondrial indices was accompanied by reduced apoptosis-related signaling. In the present study, septic stimulation altered the balance between pro-apoptotic and anti-apoptotic proteins, whereas Apelin-13 partially restored this balance and reduced downstream apoptotic activation. These results suggest that the effects of Apelin-13 on ER and mitochondrial homeostasis may converge on the regulation of cardiomyocyte survival. However, because apoptosis was not directly manipulated, it remains uncertain whether reduced apoptosis was a primary effect of Apelin-13 or a secondary consequence of alleviated ER and mitochondrial stress. In addition, Apelin-13 reduced myocardial MLKL immunoreactivity in CLP-treated rats. Activation of RIPK1/RIPK3/MLKL-related signaling has been implicated in septic myocardial injury, and disturbance of membrane lipid homeostasis has been shown to affect both necroptosis and apoptosis [36]. Inhibition of RIPK1-dependent necroptosis has also been associated with reduced myocardial inflammation and injury during sepsis [37].

The consistency between the CLP rat model and LPS-challenged H9c2 cells further supports the potential protective effect of Apelin-13. The CLP model reproduces important features of polymicrobial sepsis, including systemic inflammation, circulatory disturbance, and interactions among multiple organs and cell populations. In contrast, the cellular model allowed the direct effects of Apelin-13 on cardiomyocyte-like cells to be evaluated under a relatively controlled inflammatory stimulus. Previous research has demonstrated that Apelin-13 activates survival-related ERK1/2 and Akt signaling in H9c2 cells [38].

Although the present study provides several relevant findings, a number of limitations should be acknowledged. First, an APJ knockdown or receptor-deficient model was not used; consequently, whether the observed effects of Apelin-13 were entirely dependent on APJ activation could not be determined. Second, echocardiography was not performed, and long-term survival was not evaluated. Thus, conclusions regarding recovery of cardiac function or improvement in prognosis cannot be drawn. Third, only male rats were included, and possible sex-dependent responses to Apelin-13 remain unknown. Finally, pathway-specific inhibitors and rescue experiments were not conducted. Further studies are therefore required to determine whether ER stress, mitochondrial dysfunction, apoptosis, and MLKL-associated signaling represent parallel responses or mechanistically connected components of Apelin-13-mediated protection.

Conclusion

Apelin-13 attenuated myocardial and cardiomyoblast injury in experimental sepsis. These effects were accompanied by reduced inflammation, oxidative stress, ER stress-related protein abundance, apoptosis-related changes, and MLKL expression, together with preservation of mitochondrial membrane potential. These findings support further investigation of pelin-13 in sepsis-associated myocardial injury. Studies incorporating APJ-specific interventions, direct cardiac functional assessment, and pharmacokinetic optimization are required to clarify the underlying mechanisms and translational potential.

Declarations

Competing interests

The authors declare no competing interests.

Ethics approval

All animal procedures were approved by the Institutional Animal Care and Use Committee of Dalian Medical University (approval no. AEE23119) and were conducted in accordance with the approved protocols and institutional guidelines.

Clinical Trial Number

Not applicable.

Consent to participate

Not applicable.

Consent for publication

Not applicable.

Funding

This work was supported by the Dalian City Dengfeng Program (Grant No. DF2022043); Dalian City Life and Health Guidance Plan Project (Grant No. 2023C036); WuJieping Medical Fund Project (Grant No. 320.6750.2025-01-21).

Author Contribution

Qing Song and You-Xiong Zhao: Conceptualization, Methodology, Investigation, Formal analysis, Writing – original draft. Jiu-Qing Li: Data Curation, Investigation, Validation. Zhi-Yao Fang: Software, Visualization, Data Curation. Su-Wei Li: Conceptualization, Supervision, Project administration, Funding acquisition, Writing – review & editing.

Data availability

The datasets generated and/or analyzed during the current study are available from the corresponding author on reasonable request.

References

1. Singer, M., C. S. Deutschman, and C. W. Seymour et al. 2016. The Third International Consensus Definitions for Sepsis and Septic Shock (Sepsis-3). *Journal Of The American Medical Association* 315(8):801–810. https://doi.org/10.1001/jama.2016.0287
2. Rudd, K. E., S. C. Johnson, and K. M. Agesa et al. 2020. Global, regional, and national sepsis incidence and mortality, 1990–2017: Analysis for the Global Burden of Disease Study. *Lancet* 395(10219):200–211. https://doi.org/10.1016/S0140-6736(19)32989-7
3. Hollenberg, S. M., and M. Singer. 2021. Pathophysiology of sepsis-induced cardiomyopathy. *Nature Reviews. Cardiology* 18(6):424–434. https://doi.org/10.1038/s41569-020-00492-2
4. Lukić, I., D. Mihić, and S. C. Varžić et al. 2024. Septic cardiomyopathy. *Reviews In Cardiovascular Medicine* 25(1):23. https://doi.org/10.31083/j.rcm2501023
5. Hasegawa, D., Y. Ishisaka, and T. Maeda et al. 2023. Prevalence and prognosis of sepsis-induced cardiomyopathy: A systematic review and meta-analysis. *Journal Of Intensive Care Medicine* 38(9):797–808. https://doi.org/10.1177/08850666231180526
6. Zhang, G. et al. 2022. Molecular mechanisms of cardiomyocyte death in sepsis. *Molecular Medicine Reports* 26(3):257. https://doi.org/10.3892/mmr.2022.12773

7. Tatemoto, K., M. Hosoya, and Y. Habata et al. 1998. Isolation and characterization of a novel endogenous peptide ligand for the human APJ receptor. *Biochemical And Biophysical Research Communications* 251(2):471–476. https://doi.org/10.1006/bbrc.1998.9489
8. Shin, K., C. Kenward, and J. K. Rainey. 2018. Apelinergic system structure and function. *Compr Physiol* 8(1):407–450. https://doi.org/10.1002/cphy.c170028
9. Read, C., C. M. Fitzpatrick, and P. Yang et al. 2019. International Union of Basic and Clinical Pharmacology. CVII. Structure and pharmacology of the apelin receptor with a recommendation that Elabela/Toddler is a second endogenous peptide ligand. *Pharmacological Reviews* 71(4):467–502. https://doi.org/10.1124/pr.119.017533
10. Wang, X., L. Zhang, P. Li, Y. Zheng, Y. Yang, and S. Ji. 2022. Apelin/APJ system in inflammation. *International Immunopharmacology* 109:108822. https://doi.org/10.1016/j.intimp.2022.108822
11. Song, Q., X. Wang, Z. Cao, C. Xin, J. Zhang, and S. Li. 2024. The Apelin/APJ system: A potential therapeutic target for sepsis. *J Inflamm Res* 17:313–330. https://doi.org/10.2147/JIR.S436169
12. Pan, C. S., X. Teng, and J. Zhang et al. 2010. Apelin antagonizes myocardial impairment in sepsis. *Journal Of Cardiac Failure* 16(7):609–617. https://doi.org/10.1016/j.cardfail.2010.02.002
13. Chagnon, F., D. Coquerel, and D. Salvail et al. 2017. Apelin compared with dobutamine exerts cardioprotection and extends survival in a rat model of endotoxin-induced myocardial dysfunction. *Critical Care Medicine* 45(4):e391–e398. https://doi.org/10.1097/CCM.0000000000002097
14. Luo, Q., G. Liu, G. Chen, D. Guo, L. Xu, M. Hang, and M. Jin. 2018. Apelin protects against sepsis-induced cardiomyopathy by inhibiting the TLR4 and NLRP3 signaling pathways. *International Journal Of Molecular Medicine* 42(2):1161–1167. https://doi.org/10.3892/ijmm.2018.3665
15. Coquerel, D., J. Lamoureux, and F. Chagnon et al. 2021. Apelin-13 in septic shock: Effective in supporting hemodynamics in sheep but compromised by enzymatic breakdown in patients. *Scientific Reports* 11(1):22770. https://doi.org/10.1038/s41598-021-02087-4
16. Cao, Z., W. Li, and Z. Shao et al. 2024. Apelin ameliorates sepsis-induced myocardial dysfunction via inhibition of NLRP3-mediated pyroptosis of cardiomyocytes. *Heliyon* 10(3):e24568. https://doi.org/10.1016/j.heliyon.2024.e24568
17. Salvail, W., D. Salvail, F. Chagnon, and O. Lesur. 2024. Apelin-13 administration allows for norepinephrine sparing in a rat model of cecal ligation and puncture-induced septic shock. *Intensive Care Med Exp* 12(1):68. https://doi.org/10.1186/s40635-024-00650-7
18. Khan, M. M., W. L. Yang, and P. Wang. 2015. Endoplasmic reticulum stress in sepsis. *Shock (Augusta, Ga.)* 44(4):294–304. https://doi.org/10.1097/SHK.0000000000000425
19. Vivas, W., and S. Weis. 2022. Tidy up—The unfolded protein response in sepsis. *Frontiers In Immunology* 13:980680. https://doi.org/10.3389/fimmu.2022.980680
20. Li, L., X. Peng, L. Guo, Y. Zhao, and Q. Cheng. 2020. Sepsis causes heart injury through endoplasmic reticulum stress-mediated apoptosis signaling pathway. *Int J Clin Exp Pathol* 13(5):964–971.
21. Yang, Y. P., J. Q. Zhao, and H. B. Gao et al. 2021. Tannic acid alleviates lipopolysaccharide-induced H9c2 cell apoptosis by suppressing reactive oxygen species-mediated endoplasmic reticulum

stress. *Molecular Medicine Reports* 24(1):535. https://doi.org/10.3892/mmr.2021.12174

22. Weinlich, R., A. Oberst, H. M. Beere, and D. R. Green. 2017. Necroptosis in development, inflammation and disease. *Nature Reviews Molecular Cell Biology* 18(2):127–136. https://doi.org/10.1038/nrm.2016.149
23. Wang, H., L. Sun, and L. Su et al. 2014. Mixed lineage kinase domain-like protein MLKL causes necrotic membrane disruption upon phosphorylation by RIP3. *Molecular Cell* 54(1):133–146. https://doi.org/10.1016/j.molcel.2014.03.003
24. Carbone, F., L. Liberale, A. Preda, T. H. Schindler, and F. Montecucco. 2022. Septic cardiomyopathy: From pathophysiology to the clinical setting. *Cells* 11(18):2833. https://doi.org/10.3390/cells11182833
25. Habimana, R., I. Choi, H. J. Cho, D. Kim, K. Lee, and I. Jeong. 2020. Sepsis-induced cardiac dysfunction: A review of pathophysiology. *Acute Crit Care* 35(2):57–66. https://doi.org/10.4266/acc.2020.00248
26. Boissier, F., and N. Aissaoui. 2022. Septic cardiomyopathy: Diagnosis and management. *J Intensive Med* 2(1):8–16. https://doi.org/10.1016/j.jointm.2021.11.004
27. Chen, Y., X. Teng, Z. Hu, D. Tian, S. Jin, and Y. Wu. 2021. Hydrogen sulfide attenuated sepsis-induced myocardial dysfunction through TLR4 pathway and endoplasmic reticulum stress. *Frontiers In Physiology* 12:653601. https://doi.org/10.3389/fphys.2021.653601
28. Tao, J., W. Zhu, and Y. Li et al. 2011. Apelin-13 protects the heart against ischemia-reperfusion injury through inhibition of ER-dependent apoptotic pathways in a time-dependent fashion. *American Journal Of Physiology Heart And Circulatory Physiology* 301(4):H1471–H1486. https://doi.org/10.1152/ajpheart.00097.2011
29. Li, Y., H. Lu, and W. Xu et al. 2021. Apelin ameliorated acute heart failure via inhibiting endoplasmic reticulum stress in rabbits. *Amino Acids* 53(3):417–427. https://doi.org/10.1007/s00726-021-02955-3
30. Boal, F., A. Timotin, and J. Roumegoux et al. 2016. Apelin-13 administration protects against ischaemia/reperfusion-mediated apoptosis through the FoxO1 pathway in high-fat diet-induced obesity. *British Journal Of Pharmacology* 173(11):1850–1863. https://doi.org/10.1111/bph.13485
31. Lv, S., Y. Feng, Q. Jiang, X. Lv, and Y. Yang. 2021. Relationship between Apelin/APJ signaling, oxidative stress, and diseases. *Oxid Med Cell Longev* 2021:8866725. https://doi.org/10.1155/2021/8866725
32. Kuroshima, T., S. Kawaguchi, and M. Okada. 2024. Current perspectives of mitochondria in sepsis-induced cardiomyopathy. *International Journal Of Molecular Sciences* 25(9):4710. https://doi.org/10.3390/ijms25094710
33. Salami, O. M., O. Habimana, J. F. Peng, and G. H. Yi. 2024. Therapeutic strategies targeting mitochondrial dysfunction in sepsis-induced cardiomyopathy. *Cardiovascular Drugs And Therapy* 38(1):163–180. https://doi.org/10.1007/s10557-022-07354-8

34. Song, C., Y. Zhang, and Q. Pei et al. 2022. HSP70 alleviates sepsis-induced cardiomyopathy by attenuating mitochondrial dysfunction-initiated NLRP3 inflammasome-mediated pyroptosis in cardiomyocytes. *Burns Trauma* 10:tkac043. https://doi.org/10.1093/burnst/tkac043
35. Chen, T., L. Ye, and J. Zhu et al. 2024. Inhibition of pyruvate dehydrogenase kinase 4 attenuates myocardial and mitochondrial injury in sepsis-induced cardiomyopathy. *Journal Of Infectious Diseases* 229(4):1178–1188. https://doi.org/10.1093/infdis/jiad365
36. Hu, S., M. Huang, and S. Mao et al. 2023. Serinc2 deficiency exacerbates sepsis-induced cardiomyopathy by enhancing necroptosis and apoptosis. *Biochemical Pharmacology* 218:115903. https://doi.org/10.1016/j.bcp.2023.115903
37. Zhou, H., H. Gong, and H. Liu et al. 2024. Erbin alleviates sepsis-induced cardiomyopathy by inhibiting RIPK1-dependent necroptosis through activating the PKA/CREB pathway. *Cellular Signalling* 123:111374. https://doi.org/10.1016/j.cellsig.2024.111374
38. Yin, L., P. Zhang, and C. Li et al. 2018. Apelin-13 promotes cell proliferation in the H9c2 cardiomyoblast cell line by triggering extracellular signal-regulated kinase 1/2 and protein kinase B phosphorylation. *Molecular Medicine Reports* 17(1):447–451. https://doi.org/10.3892/mmr.2017.7919

Figures

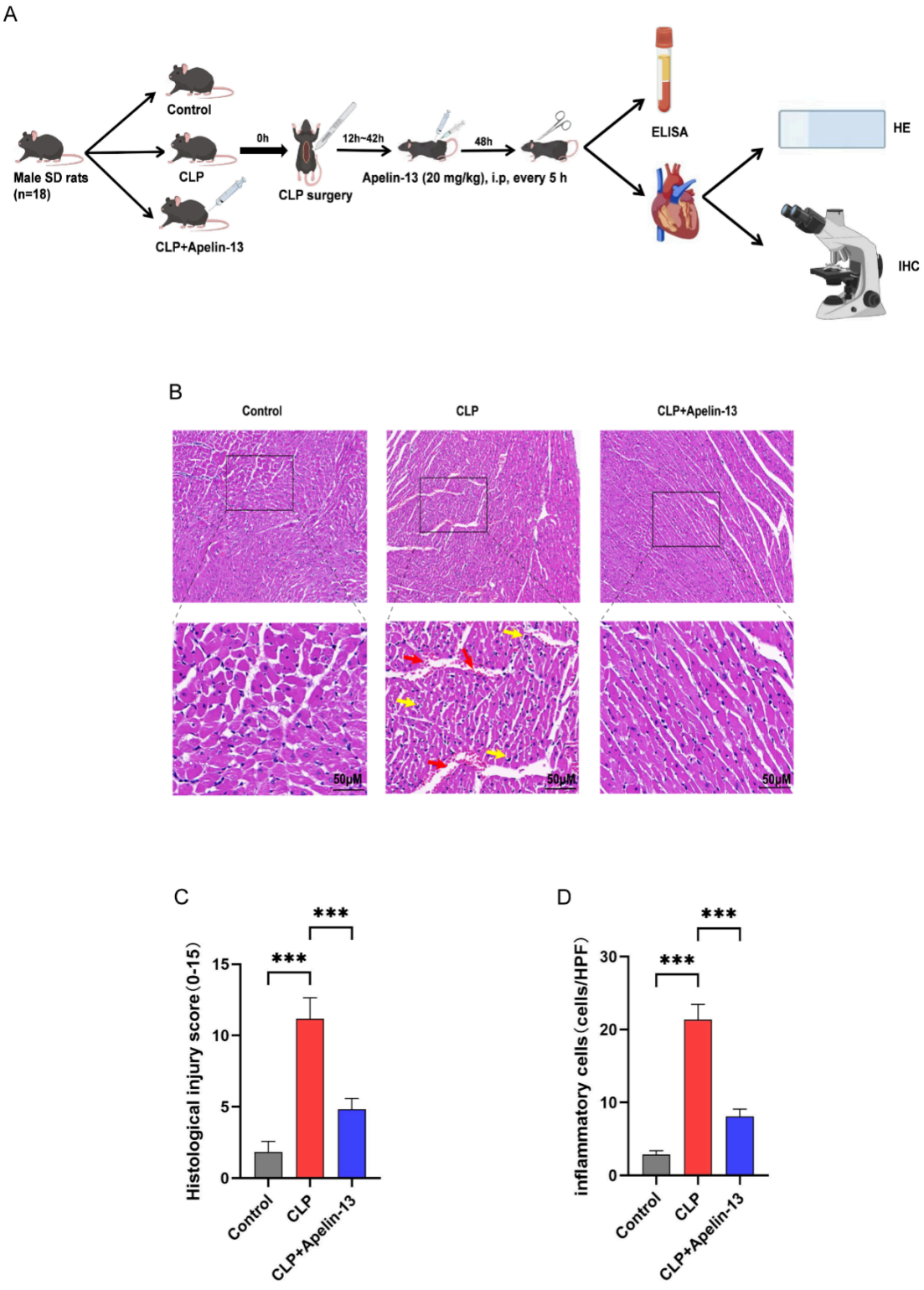


Figure 1

Apelin-13 attenuated CLP-induced myocardial injury in septic rats. (A) Experimental design. Male Sprague-Dawley rats were assigned to the Control (sham-operated), CLP, and CLP + Apelin-13 groups (n = 6 per group). Apelin-13 (20 mg/kg, intraperitoneally) was administered at 12, 17, 22, 27, 32, 37, and 42 h after CLP. Blood and heart tissues were collected at 48 h. (B) Representative hematoxylin and eosin-stained myocardial sections. Boxed areas in the upper panels are shown at higher magnification below.

Red arrows indicate myocardial fiber disruption and interstitial edema; yellow arrows indicate inflammatory cell infiltration. Scale bars, 50 μm. (C) Myocardial histological injury scores assessed using a study-defined semiquantitative scale ranging from 0 to 12. (D)Mean number of morphologically identifiable inflammatory cells per field at ×200 magnification. Each animal contributed one value obtained by averaging measurements from three non-overlapping fields. Data are mean ± SD. One-way ANOVA with Bonferroni's multiple-comparisons test; ***P < 0.001

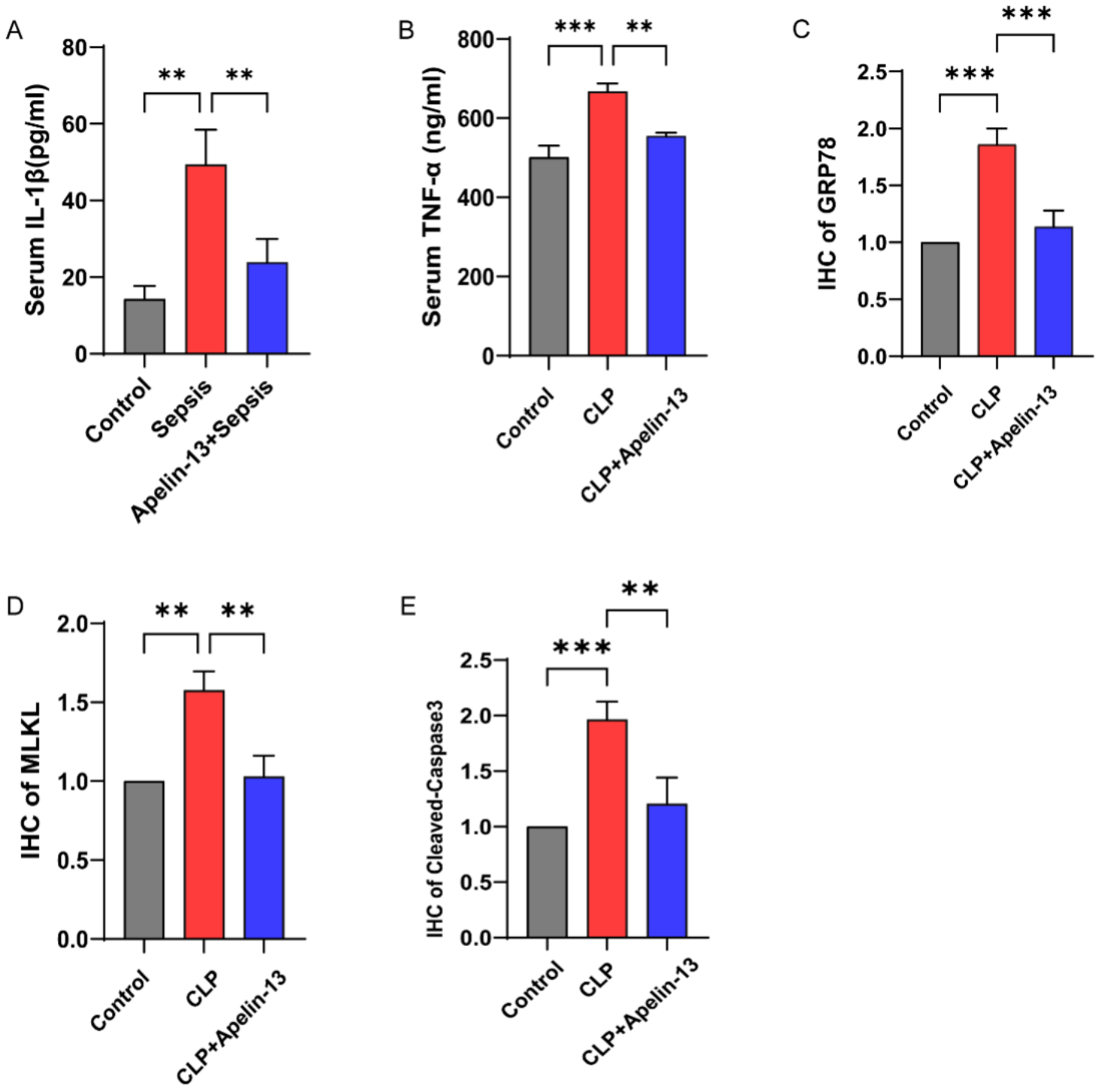


Figure 2

Apelin-13 reduced circulating pro-inflammatory cytokines and myocardial stress- and cell-death-related markers in septic rats. (A, B) Serum interleukin-1β (IL-1β) and tumor necrosis factor-α (TNF-α) concentrations measured by ELISA. (C-E) Quantification of myocardial immunohistochemical staining for glucose-regulated protein 78 (GRP78), mixed lineage kinase domain-like protein (MLKL), and cleaved caspase-3, respectively. Values are expressed relative to the Control group. n = 6 rats per group. Data are mean ± SD. One-way ANOVA with Bonferroni's multiple-comparisons test; **P < 0.01 and ***P < 0.001

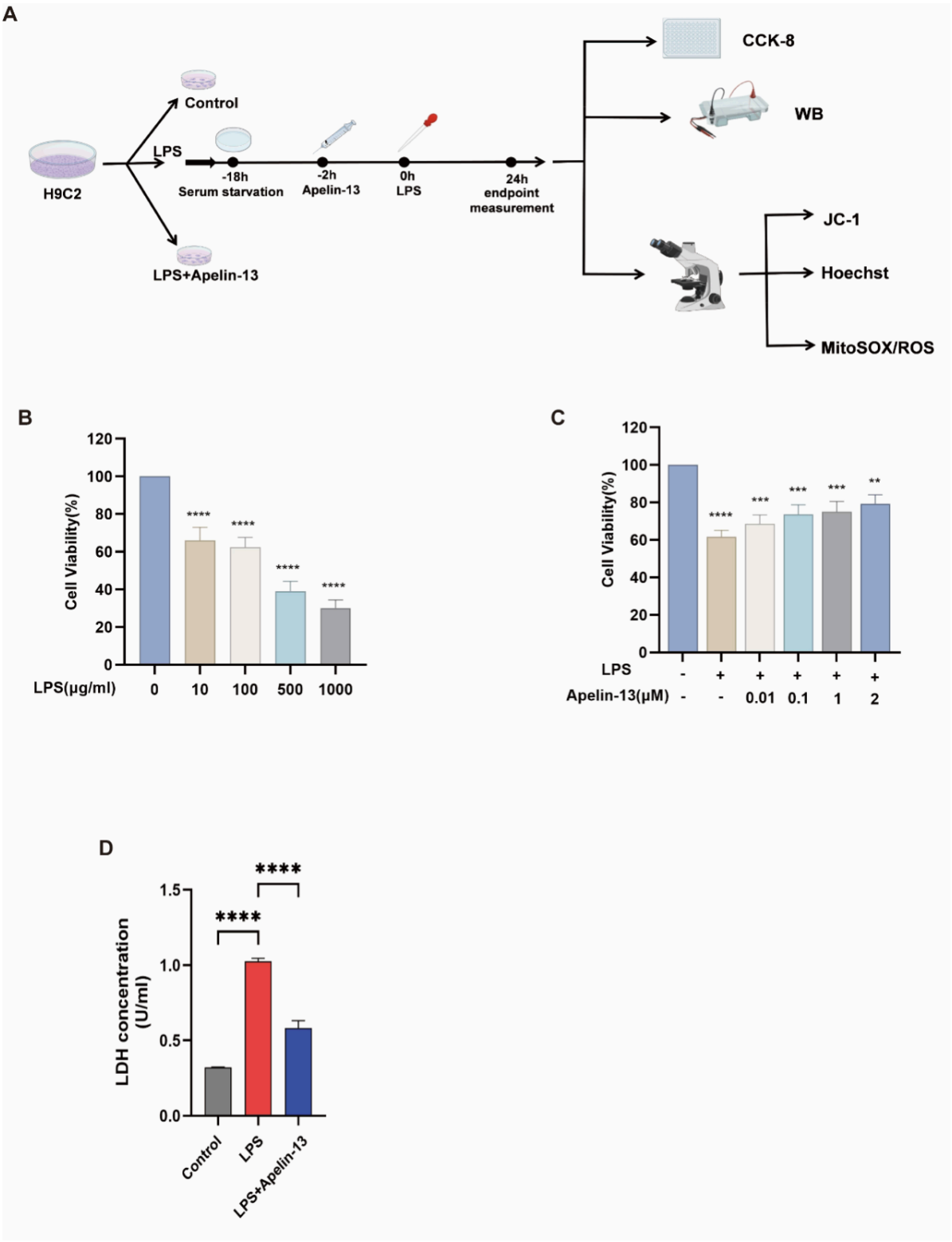


Figure 3

Apelin-13 improved viability and reduced injury in LPS-treated H9c2 cardiomyoblasts. (A) In vitro experimental protocol. Cells were serum-starved for 18 h, pretreated with Apelin-13 for 2 h, and challenged with lipopolysaccharide (LPS) for 24 h. (B) Effects of LPS (0, 10, 100, 500, and 1,000 μg/mL) on cell viability measured using the CCK-8 assay. (C) Effects of Apelin-13 (0.01, 0.1, 1, and 2 μM) on viability after LPS challenge. (D) Lactate dehydrogenase (LDH) in culture supernatants. n = 3 independent biological experiments. Data are mean ± SD. One-way ANOVA with Bonferroni's multiple-comparisons test; **P < 0.01, ***P < 0.001, and ****P < 0.0001

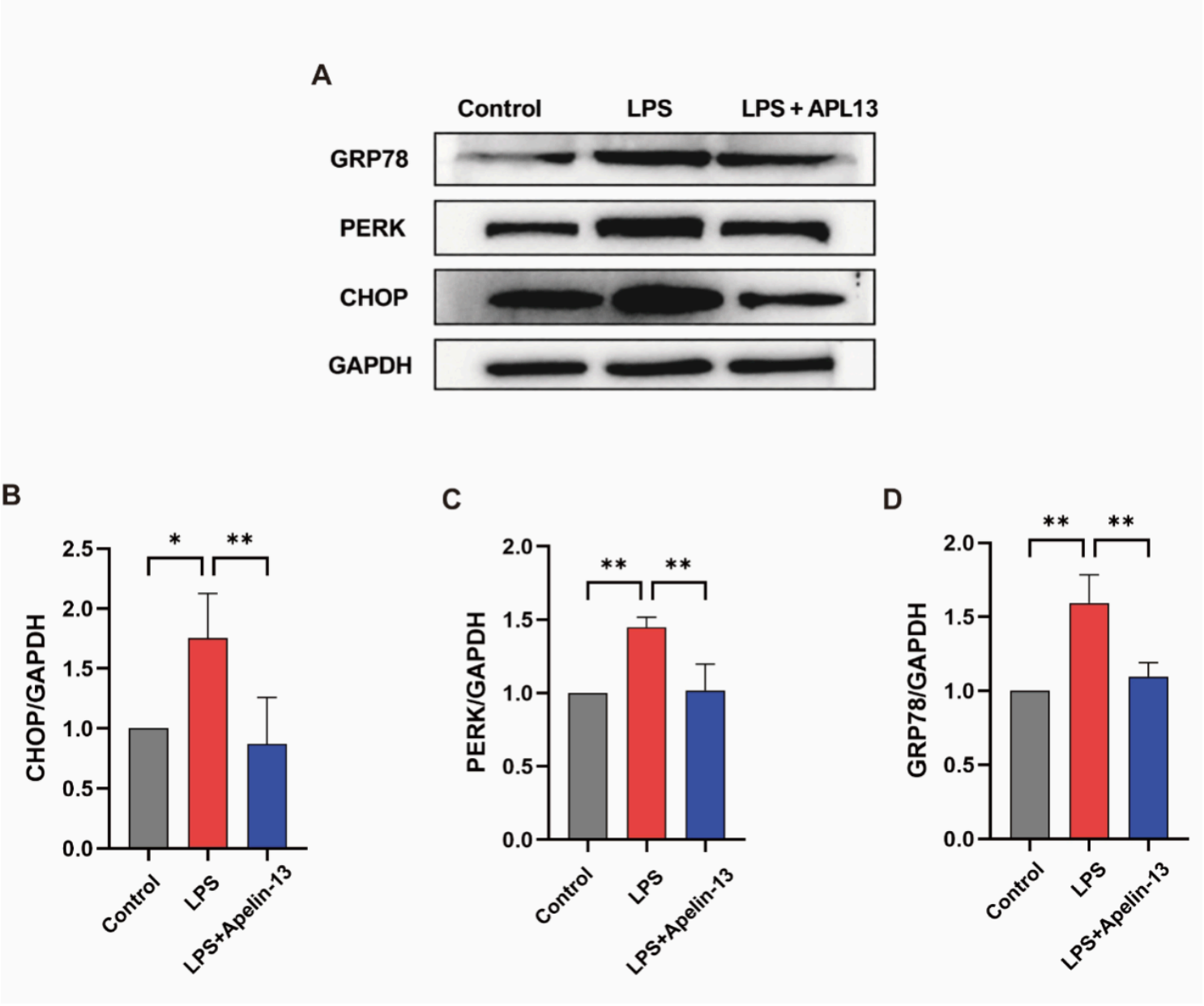


Figure 4

Apelin-13 reduced ER-stress-related protein abundance in LPS-challenged H9c2 cells. (A) Representative western blots for glucose-regulated protein 78 (GRP78), protein kinase R-like endoplasmic reticulum

kinase (PERK), C/EBP homologous protein (CHOP), and GAPDH. (B-D) Densitometric quantification of CHOP, PERK, and GRP78 normalized to GAPDH. n = 3 independent biological experiments. Data are mean ± SD. One-way ANOVA with Bonferroni's multiple-comparisons test; *P < 0.05 and **P < 0.01

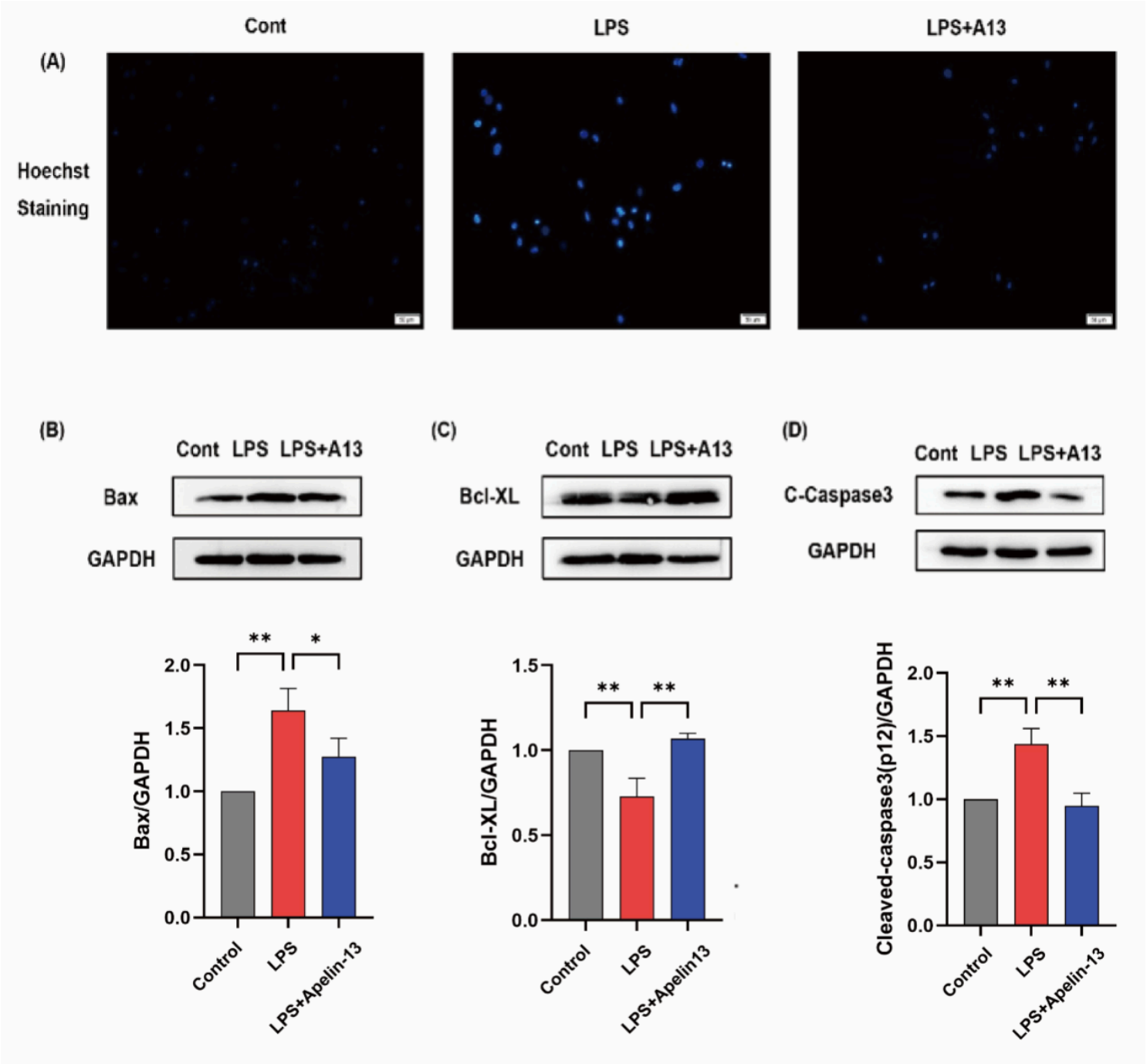


Figure 5

Apelin-13 attenuated apoptosis-related changes in LPS-challenged H9c2 cells. (A) Representative Hoechst 33342 fluorescence images. (B-D) Representative western blots and densitometric analyses of Bax, Bcl-xL, and cleaved caspase-3, respectively. Protein abundance was normalized to GAPDH. Scale bars are shown in the images. n = 3 independent biological experiments. Data are mean ± SD. One-way ANOVA with Bonferroni's multiple-comparisons test; *P < 0.05 and **P < 0.01

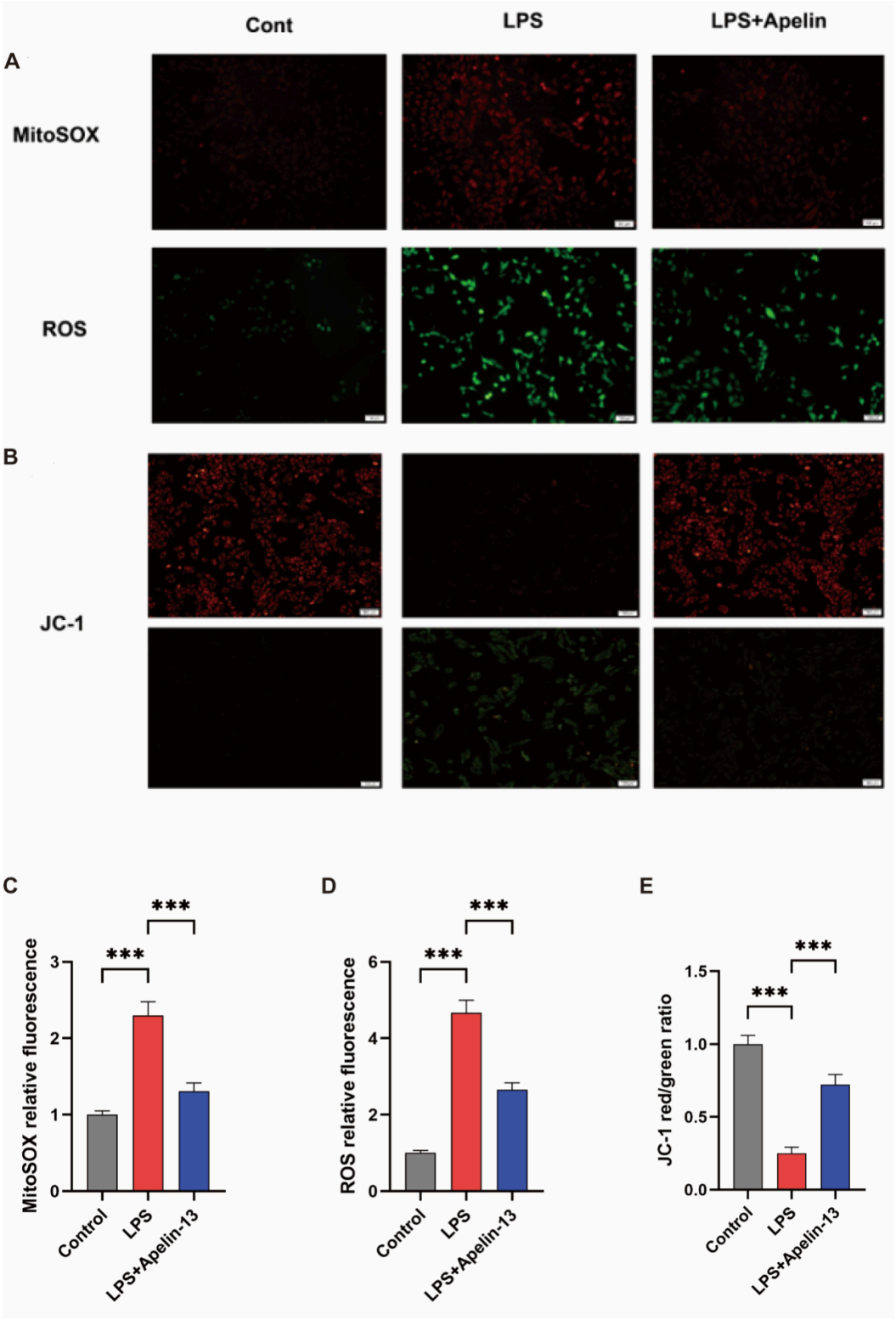


Figure 6

Apelin-13 suppressed oxidative stress and preserved mitochondrial membrane potential in LPS-challenged H9c2 cells. (A) Representative images of mitochondrial superoxide and intracellular reactive oxygen species detected using MitoSOX Red and a general ROS-sensitive probe, respectively. (B) Representative JC-1 fluorescence images. JC-1 aggregates exhibit red fluorescence, whereas JC-1 monomers exhibit green fluorescence. (C) Relative MitoSOX fluorescence. (D) Relative intracellular ROS

fluorescence. (E) JC-1 red-to-green fluorescence ratio. Scale bars are shown in the images. n = 3 independent biological experiments. Data are mean ± SD. One-way ANOVA with Bonferroni's multiple-comparisons test; ***P < 0.001

Supplementary Files

This is a list of supplementary files associated with this preprint. Click to download.

- SupplementaryUncroppedWBImages.pdf